Journal of Applied Electrochemistry **33**: 387–392, 2003.

Electrooxidation of Mn(II) to MnO_2 on graphite fibre electrodes

M.M.E. DUARTE[1,2,*], A.S. PILLA[1] and C.E. MAYER[1,2,3]
[1]*Instituto de Ingeniería Electroquímica y Corrosión, Universidad Nacional del Sur, Bahía Blanca, Argentina*
[2]*Comisión de Investigaciones Científicas de la Provincia de Buenos Aires, Argentina*
[3]*ISE Member*
*(*author for correspondence, fax: +54 291 4595182, e-mail: mduarte@criba.edu.ar)*

Received 22 April 2002; accepted in revised form 13 January 2003

Key words: carbon cloth, carbon felt, electrochemical oxidation, manganese dioxide

Abstract

Electrooxidation of Mn^{2+} to MnO_2 on carbon felt and carbon cloth electrodes (C-materials) in a weak sulfuric acid electrolyte was investigated using stationary and rotating electrodes. These materials exhibit better performance than more conventional materials such as lead. Scanning electron micrographs of the deposits show a uniform cylindrical growth of MnO_2 encapsulating the carbon fibres. The deposits spontaneously fracture following straight-lines indicating a fibrous microstructure. X-ray diffraction reveals a γ-MnO_2 structure for all deposits.

1. Introduction

Manganese dioxide and zinc are the main components of dry cells; these are the most popular source of portable electrical energy. Today, batteries do not represent a severe environmental risk, since the most common brands are manufactured with low or zero mercury, lead and cadmium contents. In many countries spent batteries are classified as household waste even though the discharge to normal landfills together with domestic waste represents a significant and continuous ingress of zinc and manganese to the soil. Common solutions are incineration or stabilization of the batteries in concrete and dumping in controlled sites [1]. However, the recycling of spent batteries would be the most convenient solution from an environmental point of view, although there are practical and economical aspects that restrict this option.

Battery recycling processes that have reached the industrial scale level are generally based on pyrometallurgical and thermal treatments [2–5]. Hydrometallurgical processes are mainly directed to zinc recovery by cathodic reduction, manganese being recovered by precipitation [6]. Electrolytic manganese recovery has been carried out in a manganese rich zinc mineral [7] but only Bartolozzi [8] gives an electrochemical procedure that permits the simultaneous recovery of manganese and zinc by a combination of anodic and cathodic processes. In consequence little is known regarding the basic aspects of electrochemical manganese recovery as MnO_2 from extracts of spent batteries.

The aim of the present work is the study of manganese oxidation to MnO_2 on cloths and felts of graphite fibres in sulfate electrolytes as a first step to develop the electrolytic recovery of manganese from spent battery liquors.

Electrolytic manganese dioxide (EMD) is usually manufactured by anodic oxidation of manganese sulfate on inert anode substrates such as titanium, lead or graphite in hot dilute sulfuric acid, the EMD being formed as a thick layer on the anode during the electrolysis. In battery related research many studies have been done on MnO_2 electrolytic deposition on platinum, titanium or graphite/carbon [9–15]. The graphite fibre materials selected for this study are utilised as electrodes in electrochemical reactors because the properties of graphite are combined with a three-dimensional flexible structure. The result is a large surface area, low-cost, rugged, chemically resistant and versatile material for different electrochemical applications [16–21].

2. Experimental details

Electrochemical experiments were carried out in a conventional glass cell, at room temperature under nitrogen atmosphere. The experimental arrangement included a platinum plate counter electrode, which was separated from the principal compartment by a porous glass diaphragm, and a saturated calomel reference electrode that was located in a Luggin capillary. All potentials are referred to the standard hydrogen electrode (SHE).

Conventional electrochemical techniques were used. Potential sweeps were impressed upon the electrodes

Table 1. Types of C-material electrodes [22]

Electrode	Material	Thickness /cm	Porosity, ε	Specific surface area /cm^{-1}
C-1	Cloth	0.12	0.85	122
C-2	Cloth	0.10	0.84	124
C-3	Cloth	0.25	0.85	–
F-1	Felt	0.52	0.95	35

between 0.94 and 2.04 V, at a scan rate of 1 mV s^{-1} or lower. Stationary potentiostatic polarization curves were measured starting from the rest potential up to 2.0 V.

In unstirred solutions, rectangular electrodes of lead, titanium and graphite fibre cloths and felts (designed as C-materials) were used. For experiments with rotating electrodes, discs of glassy carbon and C-materials were used. The properties of the different C-materials are detailed in Table 1.

The test electrolytes were aqueous solutions of 0.5 M H_2SO_4 + x M $MnSO_4$, where x varied between 0.01 and 0.5. Solutions were prepared in doubly distilled water using AR grade chemicals.

Manganese ion concentrations were analysed by plasma emission spectroscopy (Shimadzu ICPS 1000 III). The deposits of MnO_2 were studied with a scanning electronic microscope (Jeol 100), equipped with an EDAX microanalysis system. MnO_2 deposits were powdered and the XRD patterns were recorded on a Philips PW 1710 X-ray diffractometer (CuK_α; 45 kV; 30 mA).

3. Results and discussion

Polarization curves of Mn^{2+} to MnO_2 oxidation obtained with glassy carbon, lead and titanium electrodes are compared with a graphite fibre cloth in Figure 1. The C-material presents better behaviour in comparison with the other metals. Although the reaction on titanium requires smaller overpotentials, much higher currents

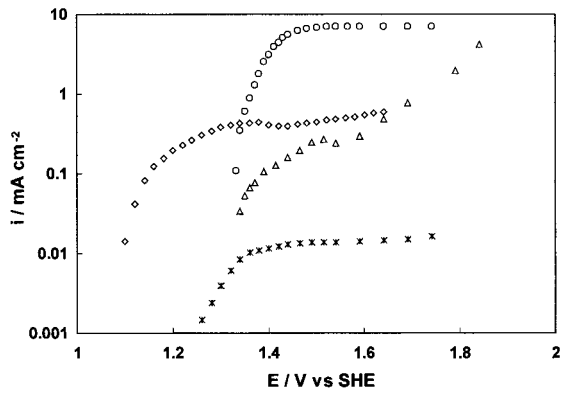

Fig. 1. Polarization curves of manganese oxidation on different electrodes. System: electrode/0.2 M $MnSO_4$ + 0.5 M H_2SO_4, Electrode: (*) glassy carbon, (Δ) Pb/PbO_2, (◇) Ti, (◯) C-2.

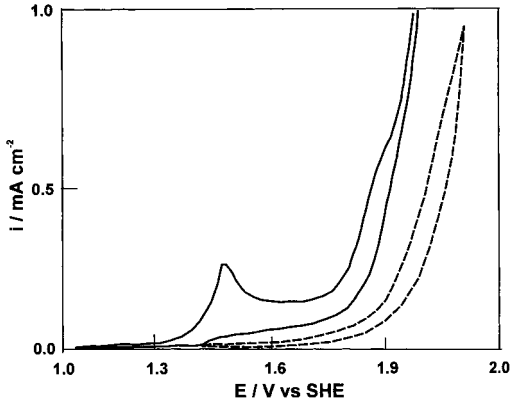

Fig. 2. Cyclic voltammograms of the systems: (- - -) glassy carbon/0.5 M H_2SO_4, (——) glassy carbon/0.2 M $MnSO_4$ + 0.5 M H_2SO_4. $|dE/dt|$=1 mV s^{-1}, rotation rate 500 rpm.

are obtained using graphite fibre electrodes. By the nature of their structure, the graphite fibres possess higher active surface areas, which are probably the origin of the higher activity.

Figure 2 shows the characteristic voltammogram of a glassy carbon electrode in 0.5 M H_2SO_4. It exhibits no remarkable features except an increase in current density at 1.9 V, which is caused by oxygen evolution. When Mn^{2+} is present, the anodic sweep shows a current increase near 1.3 V that reaches a peak at +1.45 V. Concomitant with the current increase, a dark adherent compound appears on the electrode surface, indicating the formation of MnO_2. The electrochemical deposition of MnO_2 on an inert electrode in an electrolyte containing Mn^{2+} ions occurs following the reaction [9]:

$$Mn^{2+} + 2\,H_2O \rightarrow MnO_2 + 4\,H^+ + 2\,e^- \qquad (1)$$

It is not likely that Reaction 1 occurs in a single step. The existence of a precursor such as Mn^{3+} has been suggested [11, 13, 14], originated by the following reaction:

$$Mn^{2+} \rightarrow Mn^{3+} + e^- \qquad (2)$$

Mn^{3+} can disproportionate to Mn^{2+} and Mn^{4+} at low acid concentrations, according to Reaction 3, or it may hydrolyse to form an insulating intermediate MnOOH, according to Reaction 4:

$$2\,Mn^{3+} + 2\,H_2O \rightarrow Mn^{2+} + MnO_2 + 4\,H^+ \qquad (3)$$

$$Mn^{3+} + 2\,H_2O \rightarrow MnOOH + 3\,H^+ \qquad (4)$$

Subsequently the intermediate product is oxidized to MnO_2:

$$MnOOH \rightarrow MnO_2 + H^+ + e^- \qquad (5)$$

The reduction in current density after the first peak can be attributed to the formation of the insulating intermediate, MnOOH, as suggested by Petitpierre et al.

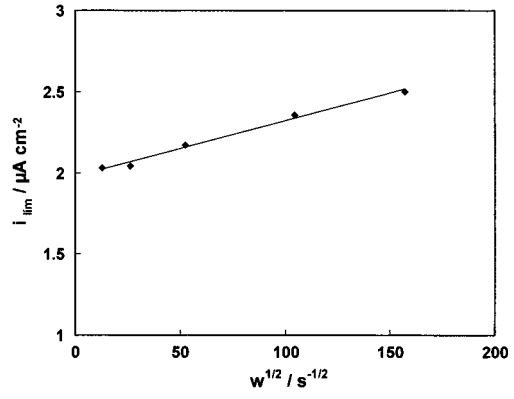

Fig. 3. Variation of the limiting current (i_{lim}) with rotation rate. System: glassy carbon/0.2 M $MnSO_4$ + 0.5 M H_2SO_4.

[11]. The shoulder at 1.8 V can be attributed to the oxidation of MnO_2 to soluble MnO_4^- ions, overlapped with oxygen evolution, leading to the formation of thinner deposits of MnO_2 at such high potentials [13].

The current always seems to approach a limiting value (i_{lim}) at high potentials before the onset of oxygen evolution, even with rotating electrodes. From experiments with rotating disk electrodes (Figure 3), it is observed that the limiting current density follows a linear relationship with respect to the square root of the rotation rate. However, extrapolation to $\omega = 0$ does not go through the origin, indicating the existence of a more complex mechanism. On the other hand, the slope is rather low and the diffusion coefficient obtained from the Levich plot [23] is of the order of 10^{-11} cm^2 s^{-1}, too small for ionic species in solution.

The cyclic voltammograms of a C-2 electrode are shown in Figure 4. The blank in absence of manganese exhibits no particular feature. When Mn^{2+} is added, a sharp anodic peak is observed at 1.45 V, and a second

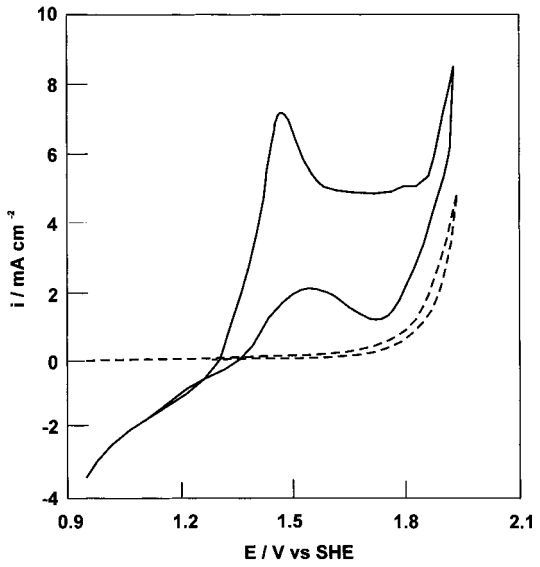

Fig. 4. Cyclic voltammograms of the systems: (- - -) C-2/0.5 M H_2SO_4: (——) C-2/0.2 M $MnSO_4$ + 0.5 M H_2SO_4. $|dE/dt|$=0.5 mV s^{-1}, rotation rate: 500 rpm.

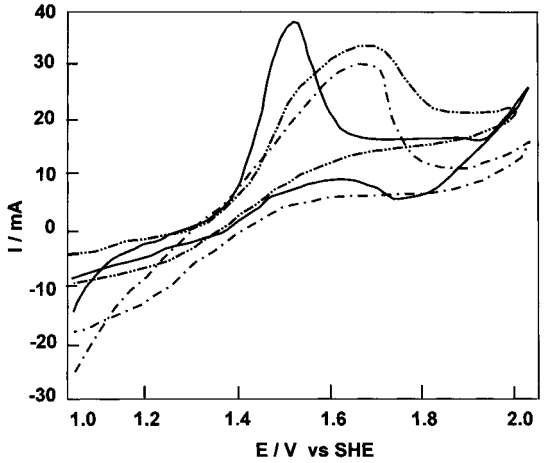

Fig. 5. Cyclic voltammograms of different graphite fibre electrodes. System: electrode/0.2 M $MnSO_4$ + 0.5 M H_2SO_4, electrode: (-••-) C-1; (—) C-2; (-•-) F-1. $|dE/dt|$=1 mV s^{-1}, rotation rate 500 rpm

smaller peak at 1.8 V, before the onset of oxygen evolution. In the cathodic sweep the negative current corresponds to MnO_2 reduction. The current densities measured with this electrode are much higher than those registered with the carbon vitreous electrode, and the features of the voltammogram are more clearly defined.

Figure 5 shows the voltammograms corresponding to the oxidation of Mn^{2+} to MnO_2 for different C-materials. A better definition of the principal anodic features, the peak at 1.45 V, and the constant current between 1.6 and 1.9 V, is observed with the thinner C-2 electrode. As the thickness of the electrode increases, the oxidation peak becomes more rounded, it moves to more positive potentials and the corresponding current diminishes. This phenomenon is more marked in a felt. Changes in the shape of voltammograms are frequent in porous electrodes, due to concentration changes and the ohmic drop in the pore electrolyte. An additional contribution may arise from the lower electrical conductivity of MnO_2.

Polarization curves for different C-materials are compared in Figure 6. The curve for a lead electrode is shown for reference. The steady-state currents increase with anodic potential near the reversible deposition potential. At high overpotentials the curves may maximize before levelling off and reaching a constant current.

Figure 7 shows polarization curves for a graphite fibre electrode in unstirred solutions of different manganese concentrations. The limiting current density plotted against manganese concentration is shown in Figure 8. i_{lim} depends on the manganese concentration following a linear relationship in the range from 0.01 to 0.2 mol L^{-1}, but the relationship becomes nonlinear for higher concentrations.

When forced convection is introduced, the manganese oxidation current on graphite fibre electrodes in steady state measurements increases by about fifteen times (Figure 9). However, this growth is independent of rotation rate, being observable from 50 rpm upward.

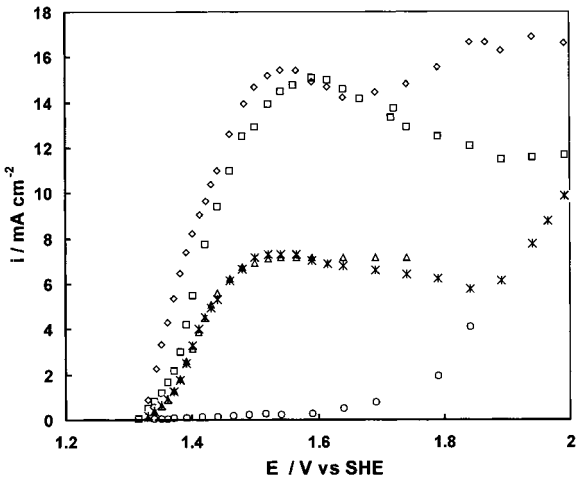

Fig. 6. Polarization curves of different materials. System: material/0.2 M $MnSO_4$ + 0.5 M H_2SO_4, unstirred electrolyte. Material: (*) C-1; (Δ) C-2; (□) C-3; (◇) F-1; (○) Pb.

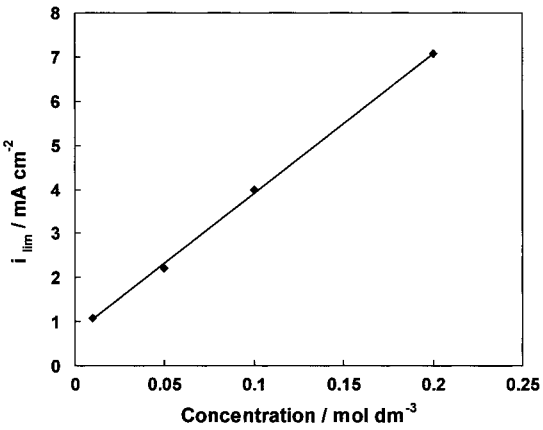

Fig. 8. i_{lim} as a function of $MnSO_4$ concentration. System: C-2/x M $MnSO_4$ + 0.5 M H_2SO_4.

When the rotation rate is increased, the current at a given potential reaches a limiting value which is independent of time and rotation rate, but increases with Mn^{2+} ion concentration.

Figures 3, 6 and 9 show a particular behaviour of the Mn^{2+}/MnO_2 system. In static electrodes the reaction seems to be under mass transfer control, but in rotating electrodes this dependence is much less significant. This behaviour may be explained if changes in the reaction mechanism are assumed. At low rotation rates the Mn^{2+} ion concentration at the surface of the MnO_2 diminishes due to slow diffusion from the bulk electrolyte. Reaction 5 becomes a fast step, compared with Reactions 3 and 4. Therefore, diffusion of Mn^{2+} to the electrode surface controls the reaction.

Under forced convection, Mn^{2+} transport to the electrode surface becomes faster than the reactions where it is consumed. MnOOH predominates on the MnO_2 surface, due to the competition of Reactions 3 and 4. The rate determining step gradually shifts to Reaction 5 [12].

Figure 10 shows the morphology of the deposits of MnO_2 on different anode materials. On plane electrodes, as in the case of lead and glassy carbon (Figure 10(a)), a relatively uniform deposit with polygon shaped particles is observed. On the other hand, the SEM micrographs of cloths reveal a relatively even distribution on the fibres with no agglomeration (Figure 10(b)). In general, the deposit is uniform and appears to encapsulate the fibres. This cylindrical growth is possibly caused by the uniform current distribution due to the additional resistance introduced by the oxide. The deposits fracture spontaneously and the fractures are remarkably straight, indicating a fibrous structure [24], the fibres running from the substrate to the growing face (Figure 10(d)). Some differences are observed between cloths and felts. On felts, protrusions from the deposit are observed (Figure 10(e) and (f)) while in cloths the deposits follow the contour of the fibres closely. The structural characteristics of both materials are the source of the differences. Cloths are constructed of bundles of fibres, while in the felts the fibres are separated and

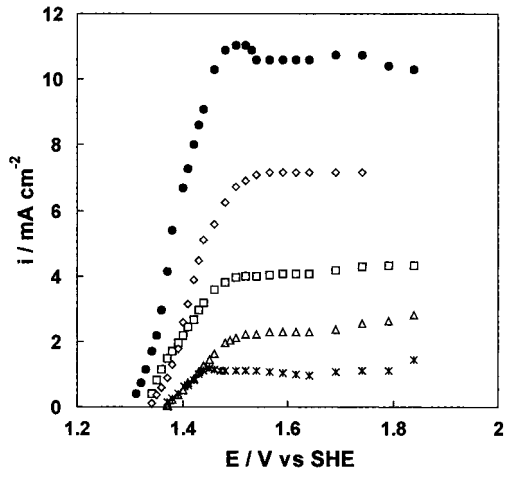

Fig. 7. Polarization curves as a function of $MnSO_4$ concentration. System: C-2/x M $MnSO_4$ + 0.5 M H_2SO_4, unstirred electrolyte. x = (*) 0.01; (Δ) 0.05; (□) 0.1; (◇) 0.2, (●) 0.5.

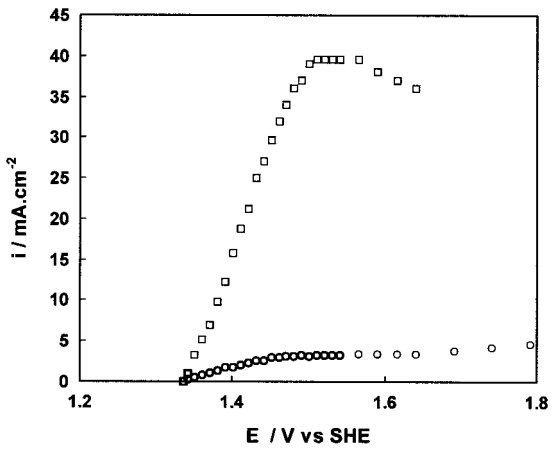

Fig. 9. Polarization curves showing the effect of forced convection. System: C-2/0.1 M $MnSO_4$ + 0.5 M H_2SO_4, (○) Unstirred electrolyte; (□) 500 rpm.

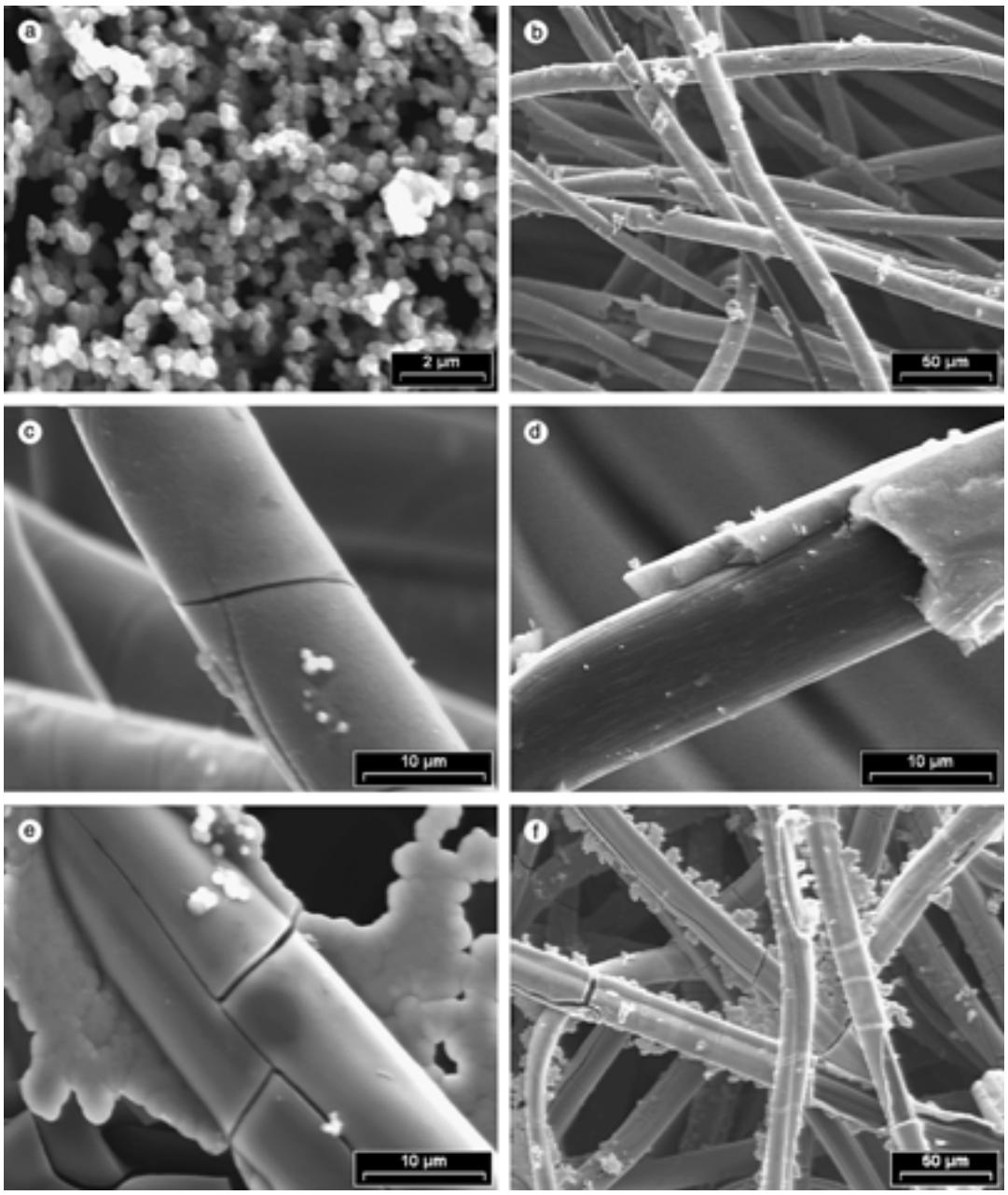

Fig. 10. Micrographs of MnO_2 deposits on different materials: (a) glassy carbon after 1 h at 1.54 V; (b, c, d) C-3 after 1 h at 1.64 V; (e–f) F-1 after 1 h at 1.64 V.

randomly distributed. In the cloths the solution is more likely to flow around the bundles than through them, since the space between the fibres of a bundle is very limited. On the other hand, in the felt the solution will be in more efficient contact with the fibres, since the inter-fibrous spaces are larger and evenly distributed. So, mass transport to the surface is more efficient.

Figure 11 shows X-ray diffraction patterns of manganese dioxide deposited over different materials after 180 min electrolysis at 1.54 or 1.64 V. For comparison, XRD patterns of synthetic graphite, chemical and electrolytic γ-MnO_2 [25] are also shown. Electrolytic γ-MnO_2 has a more diffuse pattern than the chemically prepared material, with several lines missing. Although the characteristic peak at $2\theta = 22.2°$ is scarcely visible or missing due to superposition with the graphite peak, the patterns of the different samples agree quite well with that of electrolytic γ-MnO_2. Changes in electrode material or anode potential lead to small differences in the diffraction pattern.

4. Conclusions

Graphite fibre electrodes are effective for the recovery of the manganese ions from acid solutions. Using graphite fibre cloth or felt electrodes for the recovery

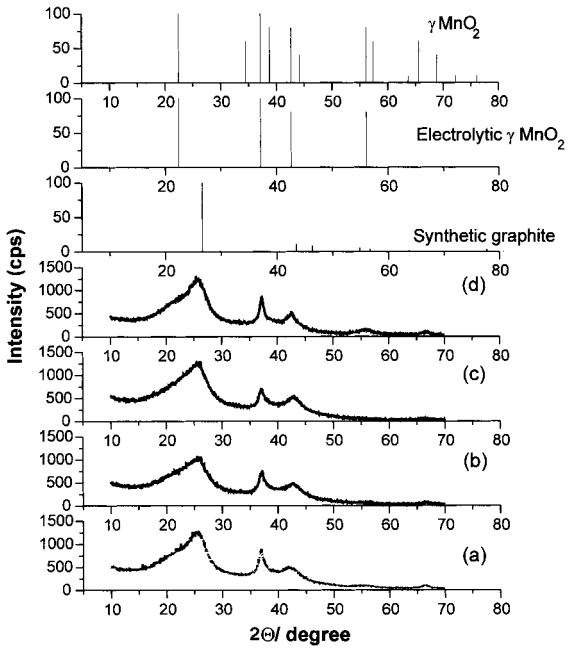

Fig. 11. XRD patterns of manganese dioxide obtained for 180 min. (a) C-1 at $E = 1.64$ V; (b) F-1 at $E = 1.64$ V; (c) F-1 at $E = 1.54$ V; (d) C-1 at $E = 1.54$ V.

of manganese as MnO_2, higher currents than in the case of the lead electrode were obtained at the same anodic potential.

The deposits show a uniform cylindrical growth of MnO_2 which encapsulates the graphite fibres. MnO_2 deposits fracture spontaneously and the fractures are remarkably straight, indicating a fibrous structure. X-ray diffraction results identify MnO_2 deposits as γ-MnO_2.

Acknowledgement

Grateful acknowledgement is made to the Universidad Nacional del Sur and the Comisión de Investigaciones Científicas de la Provincia de Buenos Aires for support of this work.

References

1. J-P. Wiaux and J-P. Waefler, *J. Power Sources* **57** (1995) 61.
2. T. Kanemura and T. Matsuoka, *J. Power Sources* **57** (1995) 23.
3. R. Burri and A. Weber, *J. Power Sources* **57** (1995) 31.
4. W.R. Meador, *J. Power Sources* **57** (1995) 37.
5. P. Ammann, *J. Power Sources* **57** (1995) 41.
6. S. Fröhlich and D. Sewing, *J. Power Sources* **57** (1995) 27.
7. B. Verbaan and B. Mullinder, *Hydrometallurgy* **7** (1981) 339.
8. M. Bartolozzi, G. Brazzini, P.F. Marconi and S. Bonvini, *J. Power Sources* **48** (1994) 389.
9. K.V. Kordesch, 'Batteries (Manganese Dioxide)', Vol. 1 (Marcel Dekker, New York, 1974).
10. R.L. Paul and A. Cartwright, *J. Electroanal. Chem.* **201** (1986) 113.
11. J.Ph. Petitpierre, Ch. Comninellis and E. Plattner, *Electrochim. Acta* **35** (1990) 281.
12. W.H. Kao and V.J. Weibel, *J. Appl. Electrochem.* **22** (1992) 21.
13. S. Rodriguez, N. Munichndraiah and A.K. Shukla, *J. Appl. Electrochem.* **28** (1998) 1235.
14. S. Nijjer, J. Thonstad and G.M. Haarberg, *Electrochim. Acta* **46** (2000) 395.
15. T.N. Anderson, *in* R.E. White, B.E. Conway and J.O'M. Bockris (Eds), 'Modern Aspects of Electrochemistry', No. 30 (Plenum Press, New York, 1996), p. 313.
16. B.M. Kim and J.L. Weininger, *Environ. Prog.* **1** (1982) 121.
17. Y. Oren and A. Soffer, *Electrochim. Acta* **28** (1983) 1649.
18. F. Walsh, 'A First Course in Electrochemical Engineering' (The Electrochemical Consultancy, Romsey, UK 1993), p. 142.
19. R. Carta, S. Palmas, A.M. Polcaro and G. Tola, *J. Appl. Electrochem.* **21** (1991) 793.
20. N. Vatistas, P.F. Marconi and M. Batolozzi, *Electrochim. Acta* **36** (1991) 339.
21. E. Ayranci and B.E. Conway, *J. Appl. Electrochem.* **31** (2001) 25.
22. A.S. Pilla, E.O. Cobo and M.M.E. Duarte, Proc. IX Congreso Argentino de Fisicoquimica, San Luis, Argentina, 21–25 Nov. (1994), p. 150.
23. E. Gileadi, 'Electrode Kinetics' (VCH Publishers, New York, 1993).
24. K. Matsuki, T. Endo and H. Kamada, *Electrochim. Acta* **29** (1984) 983.
25. Joint Committee on Powder Diffraction Standards, Powder Diffraction File Sets 11–15 (revised), Philadelphia (1972).